RESEARCH ARTICLE

Applied Polymer SCIENCE **WILEY**

Production and comprehensive characterization of PVA/chitosan transdermal composite mats loaded with bioactive curcumin; evaluation of its release kinetics, antioxidant, antimicrobial, and biocompatibility features

Fatih Ciftci[1,4] | Ali Can Özarslan[2] | Nilüfer Evcimen Duygulu[3]

[1]Department of Biomedical Engineering, Fatih Sultan Mehmet Vakif University, Istanbul, Turkey

[2]Department of Bioengineering, Yildiz Technical University, Istanbul, Turkey

[3]Department of Metallurgical and Material Engineering, Yildiz Technical University, Istanbul, Turkey

[4]Department of Technology Transfer Office, Fatih Sultan Mehmet Vakif University, Istanbul, Turkey

Correspondence
Fatih Ciftci, Department of Biomedical Engineering, Fatih Sultan Mehmet Vakif University, Istanbul, Turkey.
Email: faciftcii@gmail.com; fciftci@fsm.edu.tr

Abstract

Recently, researchers have shown increasing interest in incorporating bioactive substances with therapeutic properties into fiber-structured mat biomaterials, which are favored as tissue scaffolds for wound healing applications. In this study, curcumin (Cur)-loaded polyvinyl alcohol (PVA)/chitosan (CS) composite mats were produced using the electrospinning method and followed by the freeze-drying method. Scanning electron microscope images proved the homogeneous structure of the composite mats, and Fourier transform infrared spectroscopy analysis showed that the Cur-loaded composite mats were successfully produced. The antibacterial activity of Cur-loaded PVA/CS composite mats was evaluated against *Escherichia coli* and *Staphylococcus aureus,* and the results showed that the antibacterial activity of the composite mats increased with the addition of Cur. Furthermore, the antioxidant test, release kinetics tests, and in vitro biocompatibility studies such as cytotoxicity, staining, and scratch assay of Cur-loaded PVA/CS composite mats were carried out. The results showed that adding Cur enhanced the bioactivity of PVA10/CS10 composite mats. Further, the biocompatibility findings indicated that 10Cur-PVA10/CS10 exhibited the highest viability value throughout all incubation periods compared with the other samples. Moreover, the highest rate of scratch closure on the 10Cur-PVA/10/CS10 composite mats was observed at the end of 24 h compared with the other composite mats. These findings indicate that the Cur-loaded PVA10/CS10 composite mats significantly positively impact cell migration and wound healing, making them a promising candidate as transdermal composite mats for tissue engineering and wound care applications.

KEYWORDS
biodegradable, bioengineering, biomaterials, composites, fibers

1 | INTRODUCTION

The human skin is the largest organ in the body, both protective from external factors and permeable to external and internal factors, as well as acting as a homeostatic barrier.[1-3] Thanks to its large surface area and transdermal properties, it is essential in delivering pharmacological and bioactive materials.[4-6] It also shields against potential thermal, mechanical, and chemical damage. In processes such as tissue injuries, loss, and burns, the skin cannot reach its natural healing processes. In this case, tissue engineering approaches can help the skin regain the lost skin tissue function. Tissue engineering aims to restore the skin's anatomical integrity to its native state. The primary objective of tissue engineering is to restore the skin to its inherent functionality while preserving its ability to allow the passage of oxygen and maintain moisture levels. In this particular scenario, tissue engineering involves using transdermal materials, which serve as a transient protective barrier within the wound site. This approach aims to expedite the process of wound healing while reinstating the mechanical integrity and flexibility of the skin. The transdermal biomaterial is impermeable to skin components and gives the patch flexibility. Transdermal materials bind the skin components to each other and the designed material to the skin. Transdermal biomaterials are used to increase skin permeability and maintain oxygen permeability and moisture while minimizing the risk of infection. Another aim is to minimize tissue loss by restoring lost mechanical stability.[4,7]

An ideal transdermal composite mat for tissue engineering should possess favorable mechanical, biocompatible, and biodegradable properties. Additionally, it should have the capability to facilitate cellular infiltration, adhesion, and proliferation while mimicking the characteristics of the extracellular matrix (ECM).[8] Nanofibrous scaffolds exhibit considerable potential as viable alternatives that closely resemble the inherent structure of the ECM, possess mechanical properties akin to the dermis, and possess suitable porosity and expansive surface area, hence facilitating cellular adhesion and proliferation. Composite matrices have garnered significant attention as scaffolds for tissue engineering applications due to their numerous advantages.[9]

Chitosan (CS) is a biopolymer generated from chitin, a semi-natural polysaccharide, through N-deacetylation. It is known for its biocompatibility and suitability for various applications. CS exhibits remarkable biocompatibility, biodegradation, antibacterial properties, and low immunogenicity.[10] It can be used in a wide range of application areas such as tissue engineering,[11] biosensing,[12] drug delivery,[8] wound healing, and so forth.[13] Therefore, hydrogel mixtures containing curcumin (Cur) and CS may be helpful as

functional transdermal composite mats. Furthermore, as composites can compensate for the shortcomings of single materials, various blend/composite systems have been considered transdermal composite mat materials.[14] For instance, Cur and CS materials may be mechanically and shapeably inadequate; synthetic polymers such as polyvinyl alcohol (PVA) can improve these deficiencies.[15] PVA, a polymer with a semicrystalline structure, has notable attributes such as excellent biocompatibility, favorable mechanical properties, water solubility, nontoxicity, and biodegradability. Consequently, PVA is extensively utilized in various biomedical applications.[16-18]

In recent years, Cur, an innate polyphenolic phytochemical derived from the rhizomes of the *Curcuma longa* L. plant, has garnered significant attention owing to its diverse and advantageous range of biological and pharmacological properties. These enclose antiinflammatory, anticancer, antioxidant, wound-healing, and antimicrobial effects.[19,20] Nevertheless, the broad clinical utilization of this notably effective compound in the context of cancer and various other diseases has encountered restrictions assignable to its suboptimal aqueous solubility, resulting in minimal systemic bioavailability.[20-22] Previous studies have reported efforts to enhance Cur's aqueous solubility, stability, and bioavailability by forming complexes or interactions with macromolecules, including gelatins, polysaccharides, and phospholipids.[23,24]

In this research, we developed composite mat configurations with different concentrations, using Cur as an additive component. For the first time, the fabrication of PVA/CS transdermal composite mat structures, which were loaded with Cur biomolecule in various ratios (5 and 10 wt%) and cross-linked with glutaraldehyde, was achieved through the utilization of electrospinning and freeze-drying techniques. Furthermore, comprehensive characterizations such as biocompatibility, biodegradability, antibacterial, antioxidant properties, and ability to promote fibroblast proliferation and adhesion of Cur-loaded and cross-linked transdermal composite mats as well as the release kinetic profile of transdermal composite mats were conducted in the present research.

2 | MATERIALS AND METHODS

PVA (MW = 146–186 kDa, 99% hydrolyzed), CS (glacial, 99–100%), acetic acid (AA, 100% anhydrous for analysis), glutaraldehyde (GA 50%, MW: 100.12 g/mol), and glycine were supplied from Sigma-Aldrich, USA. Cur was obtained from the Viet Nam Institute of Dietary Supplements (Viet Nam). L929 mouse fibroblast cell lines for cell culture studies were obtained from Fırat University, Faculty of Veterinary Medicine. The Dulbecco's modified

Eagle's medium (DMEM), fetal bovine serum (FBS), phosphate buffered saline (PBS) tablets, penicillin/streptomycin, and L-glutamine were bought from Amresco. Dimethylsulfoxide (DMSO), Trypsin/EDTA solution (0.25% [w/v]), and The MTT (3-(4,5-dimethyl-2-thiazole)-2,5-diphenyl-2H-tetrazolium bromide) powder were obtained from Sigma-Aldrich.

2.1 | Preparation of the solutions

Initially, a solution of PVA with a concentration of 10% (w/v) was generated by dissolving PVA in distilled water. The dissolution process occurred at 90°C and lasted approximately 2 h. The solution was stirred using a magnetic stirrer set at 400 rpm. A total of 10% CS (w/v) was added to 100 mL acetic acid solution (20%; v/v) and stirred to obtain a homogeneous solution. Thereafter, CS solution was added to the PVA solutions to get 100 mL of PVA/CS solutions and was stirred until it became a homogeneous solution. Secondly, 5% and 10% of Cur (w/v) were separately added in 100 mL PVA/CS solutions and then stirred with a magnetic stirrer until the Cur was homogenously dispersed at room temperature. To decrease the surface tension of the PVA/CS/Cur solutions before the electrospinning process, Tween-80 was added at a concentration of 3% and mixed with the solutions for approximately 15 min. Each PVA/CS/Cur solution was divided into 10 mL volumes and then stored at room temperature for electrospinning. Various studies were conducted to determine the optimum electrospinning conditions with the prepared solutions (Table 1).

2.2 | Fabrication of the Cur-loaded transdermal composite mats

The samples were fabricated using the NS24 electrospinning machine from Inovenso Co., located in Istanbul, Turkey. This machine is equipped with a single brass needle (inner diameter 1.63 mm), a high-voltage power source, and a syringe pump from 33 DDS Pump Systems, based in Holliston, USA. Fibers were collected on a metal cylinder covered with grease-proof paper. Upon setting up the apparatus, 10 mL of each solution was loaded into the syringes. Optimization of process parameters included flow rates of 0.5–1.0 and 1.5 mL/h, a needle-to-collector distance of 15 cm, and operating voltages of 10–12–15 kV. Each solution required approximately 3 h to achieve a similar thickness in the collected samples. Cur-loaded fiber samples obtained by electrospinning were produced as transdermal membranes by steam crosslinking with GA.[25] Briefly, the Cur-loaded fibers were placed in a petri dish, and a solution of 10 mL GA (25%) and 20 mL distilled water was placed in a desiccator closed with a lid for 8 h to reach the desired crosslink density level. Following that, the samples were subsequently treated with an aqueous solution of 0.1 M glycine to hinder any remaining unreacted aldehyde groups. They were then immersed in PBS for 24 h and left to dry overnight at 40°C. After the cross-linking process, the samples were freeze-dried at −80°C for 24 h to fabricate transdermal membranes. Following the freezing step, the molds were transferred to a lyophilizer, where the samples were dried for 12 h. The cross-linking process was done to improve the swelling behaviors and mechanical properties of the transdermal composite mats.

2.3 | Determination of physical and mechanical properties

The mechanical properties of composite mats were determined by a tensile test device (TA.XTPlus, Stable Microsystems, UK). It was decided to do the test at a speed of 5 mm/min using strips ($80 \times 20 \times 1$ mm^3). The mechanical properties of the composite mats and mats were determined using the stress–strain curves obtained via tensile tests. Measurements were carried out with three parallel specimens for each specimen group.

TABLE 1 The physical properties of electrospinning solutions.

Solution concentration (%)	Solution flow rate (mL/h)	Voltage applied (kV)	Viscosity (Pa s)	Electrical conductivity (μs/cm)	Surface tension (mN/m)
PVA10	0.5	10	0.81 (0.001)*	1008.4 (4.2)*	10.04 (0.38)*
PVA10/CS10	0.5	10	0.75 (0.001)*	1112.0 (7.1)*	4.55 (0.05)*
5Cur-PVA10/CS10	1.0	12	0.78 (0.003)*	1113.6 (1.7)*	6.12 (0.31)*
10Cur-PVA10/CS10	1.5	15	0.79 (0.002)*	1115.1 (4.6)*	8.38 (0.27)*

Note: Fabrication distance 15 cm; $n = 3$.

Abbreviations: Cur, curcumin; CS, chitosan; PVA, polyvinyl alcohol.

*Statistical significance level was determined as $p < 0.05$ and the parenthesis indicates standard deviation.

2.4 | Determination of morphological features via scanning electron microscopy analysis

The morphological characteristics of all the produced composite mats were analyzed using a scanning electron microscope (SEM; EVO LS 10 by ZEISS) device. The SEM was operated at 5 kV in secondary electron mode, and the images were further examined at a voltage of 10 kV. In order to ensure conductivity, a coating of gold–palladium was applied to all specimens, as the polymers did not possess this inherent feature.

2.5 | Determination of chemical bonds via Fourier-transform infrared spectroscopy analysis

Fourier-transform infrared (FT-IR) spectroscopy was conducted to analyze functional groups present in the produced composite mats. The characterization studies were carried out using a Bruker Alpha FT-IR device. A 4000–400 cm^{-1} spectral range was employed to identify and analyze the functional groups within the composite mats.

2.6 | Determination of swelling profiles and degradation behaviors of transdermal composite mats

The swelling profile of the composite mats was determined through a swelling test. In this test, PBS was used as the liquid medium, and the composite mats immersed in PBS (pH 7.4) were placed on an incubator set at 250 rpm at 37°C. The samples were removed from the buffer solution at the end of the 1st, 2nd, 3rd, 12th, 18th, and 24th hours of incubation and wet weighed. The swelling ratio of the composite mats was calculated using the following Equation (1).

$$\text{Swelling rate} = \frac{W_s - W_d}{W_d} \times 100. \tag{1}$$

The values indicating the swollen and dry weights were W_s and W_d, respectively. In order to adequately prepare for the examination, it was necessary to conduct an initial weighing of each composite mat to ascertain its initial weight (W_o). This W_o would then be compared with the final weight (W_d) obtained after the degradation test. The experiment was performed at a controlled temperature (37°C) in an oven, aiming to mimic the conditions of the human body. The degrading media, referred to as the PBS solution, was taken from the tubes every

24 h. Following that, the Eppendorf tubes, having had their caps removed, were repositioned in the oven to facilitate the composite mat drying process for an extra 24 h at a temperature of 37°C. Following the designated drying interval, the composite mats underwent reweighing. The deterioration rate was determined by using Equation (2) as follows:

$$\text{Degradation rate} = \frac{W_o - W_d}{W_o} \times 100. \tag{2}$$

2.7 | In vitro studies; the modeling of release kinetics

Standard curves were obtained using concentrations ranging from 0 to 78.25 μg/mL for Cur, and this process was repeated three times using ethanol as the solvent. To ascertain the content of transdermal composite mats' active ingredients, supernatants extracted from the composite mats were analyzed at 429 nm for Cur and 372 nm after appropriate dilutions in ethanol. Concentrations were subsequently determined by reference to the standard curves. To assess loading efficiency (LE), the weight of the dried composite fibers was carefully measured, and the LE was calculated using Equation (3).

$$\text{LE\%} = \frac{\text{Active Ingredient in Composites}}{\text{Total Weight of Dried Composites}} \times 100. \tag{3}$$

In vitro release models of Cur-loaded transdermal composite fiber mats were performed with a Franz diffusion cell. A 9 mL capacity receptor chamber was filled with dissolution medium (5% [v/v] ethanol + PBS 7.4 pH [20 mL]). The supporting membrane employed in the experiment was a cellulose acetate membrane with a diameter of 25 mm. Transdermal composite fiber mats with a diameter of 15 mm were positioned on the surface of the membrane while the receptor was maintained in continuous contact with the medium. The release profile of CUR was assessed by sampling 1 mL of PBS from the receptor medium at various time intervals, including 1, 2, 4, 8, 12, 48, and 72 h. The receptor medium was replenished with an equivalent volume of fresh medium following each sampling event. Each portion was then analyzed blank at 425 nm against a mixture of ethanol and PBS using a UV–visible spectrophotometer. Different concentration of Cur (0.025, 0.05, 0.075, 0.1, 0.2, 0.5, 0.75, and 1 g/mL) was used to generate linear calibration curves of Cur. Determining the total quantity of biomolecule released was performed by utilizing the calibration curve and then graphing it as a function of time. The release kinetic curves of transdermal composite mats were

calculated and analyzed by fitting the equations of mathematical models according to Fick's law.[8] There are various mathematical models aimed at modeling the release kinetics of bioactive substances loaded in polymeric composites.[8,11] The present work utilized release data to investigate the Cur release mechanism of transdermal composite mats. These data were analyzed using zero-order, first-order, Higuchi, and Korsmeyer-Peppas kinetic models. The optimal model and its corresponding model parameters were selected based on the evaluation of various kinetic models.

2.8 | In vitro studies; antioxidant activity of transdermal composite mats

The antioxidant activity of the transdermal composite mats was evaluated through the utilization of the 2,2-diphenyl-1-picrylhydrazyl radical (DPPH*) and 2,2′-azino-bis(3-ethylbenzothiazoline-6-sulfonic acid) (ABTS•+) radical scavenging technique. Each composite mat sample (0.005, 0.01, and 0.02 mg/mL) was submerged in of DPPH* assay (50 μM solutions) in ethanol. The reaction took place at room temperature in a dark environment. The control consisted of a DPPH* assay solution without any composite matting. After 30 min of incubation, the decrease in absorbance intensity at a wavelength of 517 nm was measured using a UV–vis spectroscopy instrument (PG T80+ UV–Vis Spectrophotometer). For the ABTS assay, a fixed amount of films were mixed with 10 mL of ABTS assay solution and read the absorbance at 734 nm after 30 min. The radical scavenging activity was calculated using Equation (4).

$$\text{Radical scavenging activity}(\%) = \left(\left(A_{\text{control}} - A_{\text{sample}} \right) / A_{\text{control}} \right) \times 100 \quad (4)$$

A_{control} and A_{sample} is the absorption of the control DPPH* or ABTS•+ of the corresponding samples, respectively.

2.9 | In vitro studies; antimicrobial efficacy of transdermal composite mats

The assessment of the antibacterial activity of transdermal composite mats involved the measurement of the inhibitory zone surrounding the samples after exposure to two different types of bacteria. A Gram-positive *Staphylococcus aureus* and a Gram-negative *Escherichia coli* bacterial strain were used in this experiment. The samples were placed on the surface of the nutritious agar media using sterilized forceps. In order to evaluate the antimicrobial efficacy of transdermal composite mats, the plates containing the samples were incubated at a temperature of 37°C for 24 h. Subsequently, the inhibitory zone's diameter was measured surrounding the composite mats.[11]

2.10 | In vitro studies; biocompatibility of transdermal composite mats

2.10.1 | Determination of cytotoxicity

The biological characterization of the composite mats was conducted using the L929 mouse fibroblast cell line. Before the experiment, all specimens underwent UV sterilization for 1 h and were subsequently placed into 96-well plates. L929 cells were seeded into each well at 1×10^4 cells/mL density on the prepared composite mats. The composite mats were then incubated with 5% CO_2 at 37°C for 7 days. The growth medium employed consisted of DMEM-low glucose, FBS, penicillin–streptomycin solution (0.5%, v/v), and L-glutamine (0.5%, v/v). In vitro cell viability assessment for the L929 mouse fibroblast cells seeded on the composite mats was performed using the MTT assay on the cell culture's first, third, and seventh days. The growth medium was removed after incubation at 37°C with 5% CO_2 for each predetermined day. Subsequently, 90 μL of fresh medium and 10 μL of MTT solution were added to each well, and the incubation was kept for 3 h. After this incubation period, the MTT solution was carefully discarded, and 200 μL of DMSO was added to dissolve the formazan crystals. The composite mats were then incubated for an additional 1 h to ensure complete dissolution. Finally, the media from the wells were taken, and the absorbance values of the solutions were measured via a Dynamic LEDETECT96 microplate reader at 540 nm.

2.10.2 | Cell line staining

DAPI (4′,6-diamidino-2-phenylindole) is a stain used to stain the cell nucleus that targets explicitly and labels cell nuclei, rendering them blue in fluorescence microscopy.[26] It is primarily used as a nuclear counterstain. The blue color of DAPI is instrumental in fluorescence microscopy because it contrasts vividly with the green, yellow, or red fluorescent probes used for other cellular structures. DAPI stains nuclei selectively and typically does not label the cytoplasm. The staining procedure involved equilibrating the samples in PBS for 5 min. A DAPI stock solution was then diluted to a concentration

of 300 nM in PBS, and the samples were incubated with this solution for approximately 3–5 min. After incubation, the samples were washed several times with PBS to remove excess dye. Finally, the stained nuclei were observed using a fluorescence microscope.[27] Dio-6 (3,3'-Dihexyloxacarbocyanine iodide) was employed in staining procedures as in previous dye methodologies.[28] The dye demonstrates selectivity in evaluating the functionality and morphology of endoplasmic reticulum function.

2.10.3 | Wound healing activity

A scratch assay was performed on a mouse fibroblast cell line to examine the produced mats' effects on in vitro cell migration and wound healing capabilities. In this study, L929 cells were grown in 24-well plates and then incubated at 37°C in a controlled atmosphere containing 5% CO_2. A p200 pipette tip was employed to generate a minor abrasion on the cellular layer, forming a linear mark. Subsequently, the cells were subjected to a washing procedure using PBS to eliminate residual debris. After washing, the cells were exposed to a culture media supplemented with extracts from the mats. Subsequently, the cells were incubated for 24 h. The scrape or wound was examined at several time points (e.g., 0, 12, and 24 h) using an inverted microscope set at a magnification of 100×. Cell migration between the scratch sites from the wound margins to fill the gap was seen using an optical microscope at 0, 12, and 24 h. The area of the wound gap was measured at the initial time point and after 12 and 24 h using the ImageJ software with the assistance of the MRI Wound Healing Tool.[29]

2.11 | Statistical analysis

The experimental data were subjected to a one-way analysis of variance using GraphPad Prism 8 software for statistical analysis. The mean values were subjected to statistical comparison using Duncan's multiple range test, with significance levels determined at a threshold of $p < 0.05$.

3 | RESULT AND DISCUSSION

3.1 | Physical and mechanical properties of transdermal composite mats

The physical properties of Cur-loaded PVA10/CS10 solutions have played an essential role in determining the morphology and size of the produced transdermal composite mats. The physical characterization results, including electrical conductivity, surface tension, and viscosity of the electrospinning solutions, are shown in Table 1. Factors required to produce smaller diameter composite mats include increased electrical conductivity, lower viscosity, and lower surface tension.[30] The electrical conductivity values of the PVA10/CS10 solution increased, whereas the viscosity values and the surface tension of the PVA10/CS10 solution decreased compared with the PVA10 solution as expected. Similar approaches have been observed in CS-loaded PVA composite nanofiber studies.[31] On the other hand, it was observed that adding Cur to the PVA10/CS10 solution increased the electrical conductivity, surface tension, and viscosity. These results obtained are in good agreement with previous studies.[32,33]

The Supplementary S2 provided photos displaying the stress–strain curve of the composite mats. The tensile performance of the transdermal composite mats is presented in Table 2. The data presented indicate that the tensile strength of PVA was lower than the mixture of PVA and CS. The pure PVA mat exhibited an average tensile strength of 52.2 ± 0.81 MPa. Moreover, including CS led to a tensile strength of 69.4 ± 1.7 MPa, demonstrating more significant variability than the sole presence of PVA. Nevertheless, the evaluation of the 5Cur-PVA10/CS10 composite resulted in a discernible enhancement in its tensile properties, as evidenced by the attainment of an average tensile strength of 74.3 ± 1.1 MPa. The findings indicated an increase in tensile strength with the augmentation of Cur content in PVA10/CS10 (98.5 ± 1.1 MPa). A mechanical study of the results mentioned above revealed that the inclusion of Cur had a beneficial effect on the tensile strength of the composite mats. The results may also be evident from the observed trend of improved strength with higher concentrations of Cur. Furthermore, it is worth noting that PVA exhibited a prefracture elongation of 10.01%.

TABLE 2 Mechanical properties of transdermal composite mats.

Samples	Tensile strength (MPa)	Strain at break (%)
PVA10	52.2 (0.81)*	10.01 (0.9)*
PVA10/CS10	69.4 (1.7)*	7.1 (0.8)*
5Cur-PVA10/CS10	74.3 (1.1)*	19.2 (1.7)*
10Cur-PVA10/CS10	98.5 (1.1)*	22.6 (1.3)*

Abbreviations: Cur, curcumin; CS, chitosan; PVA, polyvinyl alcohol.
*Statistical significance level was determined as $p < 0.05$ and the parenthesis indicates standard deviation.

FIGURE 1 Scanning electron microscope images and diameter distributions of (a) PVA10, (b) PVA10/CS10, (c) 5Cur-PVA10/CS10, and (d) 10Cur-PVA10/CS10 transdermal composite mats. (e) Comparative statistical analysis of mat samples (***statistical significance level was determined as $p < 0.05$). Cur, curcumin; CS, chitosan; PVA, polyvinyl alcohol. [Color figure can be viewed at wileyonlinelibrary.com]
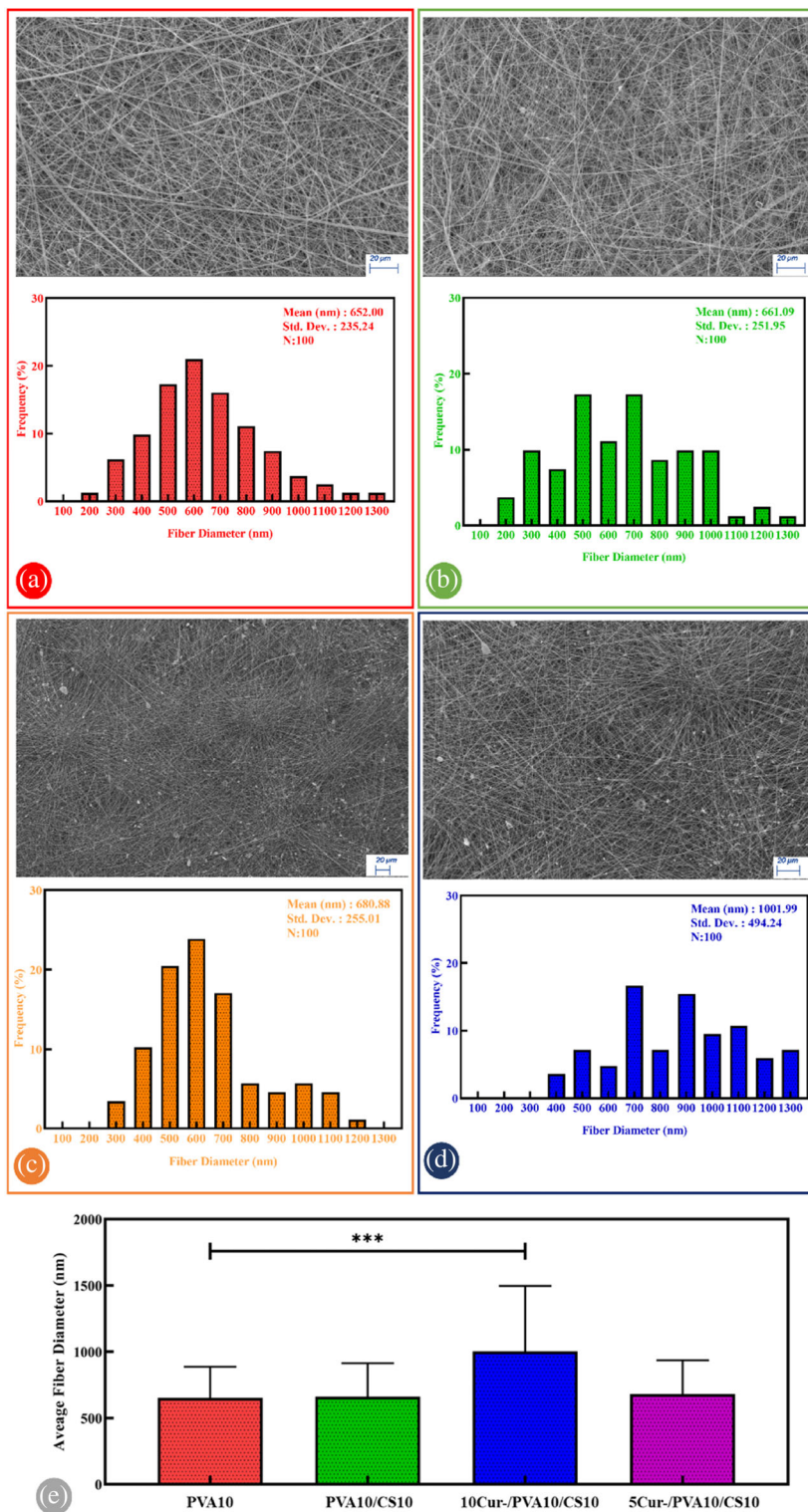
However, when CS was introduced, the elongation value decreased to 7.1%. The experimental findings demonstrated a good association between the increase of Cur concentration and the improvement of tensile strength. The strain analysis conducted at the point of fracture demonstrated that the inclusion of Cur had a favorable effect on the elasticity of the composite mats. The ideal candidate for achieving desirable mechanical qualities was identified as 10Cur-PVA10/CS10. This candidate demonstrated the highest tensile strength and strain values at the point of break among all the analyzed Cur-loaded transdermal composite mats. These results were in a good agreement with the result previously obtained in a different study, which explains the significant

improvement in mechanical analysis to the extensive crystallization. The results of this work ensure further support for the claim that Cur has a favorable effect on mechanical strength.[34,35]

3.2 | Morphological properties of transdermal composite mats

The morphological attitude of the fibers is affected by solution and process parameters. In Table 1, fabrication conditions and the solution parameters such as viscosity, electrical conductivity, and surface tension values are given. As commonly known, viscosity variation played a critical role in bead-free fiber formation and fiber diameter. An increment in viscosity leads to more significant fiber occurrence. When process parameter variations were handled, high flow rate and voltage values caused an increment in fiber diameters. According to the results, flow rate variation influenced the increase in the fiber diameter. The various diameters produced at the various solutions are shown in Figure 1. Based on the findings, it was observed that the pictures acquired were almost devoid of beads and had a uniform distribution. The average diameter of the PVA10 was determined to be 652.00 ± 235.24 nm. Figure 1a showed the SEM image of the PVA10/CS10 composite mat with diameter distribution histogram. The results showed that the PVA10/CS10 composite mat had a uniform and almost beadless morphology with a 661.09 ± 251.95 μm mean diameter value. Figure 1b illustrates the morphological characteristics of the transdermal composite mat containing Cur-loaded PVA10/CS10. The average diameter distributions were analyzed, and the findings indicated that the addition of CUR did not significantly alter the morphology of the PVA10/CS10 composite mat. In the previous PVA/CS nanofiber study in the literature, the diameter of the fiber was randomly observed as 279.843 nm.[36] The fiber diameters of the 5Cur-PVA10/CS10 were obtained as 680.88 ± 255.01 μm (Figure 1c). In similar PVA/Cur studies, "beading" was observed in fiber diameters, and fiber diameter was measured as 350 nm.[32] The 10Cur-PVA10/CS10 had a 1001.99 ± 491.24 μm mean diameter value with smooth and homogeneous morphology (Figure 1d). In a similar PVA/CS/Cur nanofiber study, the Cur-loaded PVA/CS fiber measurement was observed as 1250 ± 430 nm.[34] SEM image of the 10Cur-PVA10/CS10 transdermal composite mat revealed almost beadless structure that exhibited mild distortion. Additionally, the fibers inside the mat exhibited a transformation into bead-like structures. The findings of this study demonstrated that the inclusion of Cur resulted in a reduction in the diameter of the transdermal composite mats.

However, it was observed that a higher Cur ratio may led to the formation of a bead-like morphology.

3.3 | Functional groups of transdermal composite mats

The FT-IR spectra of PVA, CS, Cur, and the transdermal composite mats (PVA10/CS10, 5Cur/PVA10/CS10, and 10Cur/PVA10/CS10) are presented in Figure 2. The PVA spectrum has distinct peaks corresponding to several functional groups. These include the —OH group at 3319 cm^{-1},[34] stretching vibrations of CH$_2$ at 2941 cm^{-1}, CH groups at 2912 cm^{-1}, and C=O stretching vibrations at 1734 cm^{-1}. Additionally, deformation bands of CH$_2$ at 1435 cm^{-1}, CH at 1375 cm^{-1}, and C—O stretching vibrations at 1096 and 1258 cm^{-1} were observed.[37] The detected bands in the Cur sample at wavenumbers of 3085–3552, 1588, 1512, 1265, and 1143 cm^{-1} can be related to specific molecular vibrations. These vibrations correspond to the phenolic O—H stretching, stretching vibrations of the benzene ring, C=C vibrations, aromatic C—O stretching, and C—O—C stretching modes, respectively.[38] There is a possibility that many types of interactions may take place, wherein PVA and Cur may engage in hydrogen bonding via their hydroxyl functional groups or create ionic connections through the charged functional groups found on the molecules.[39] The ionization of
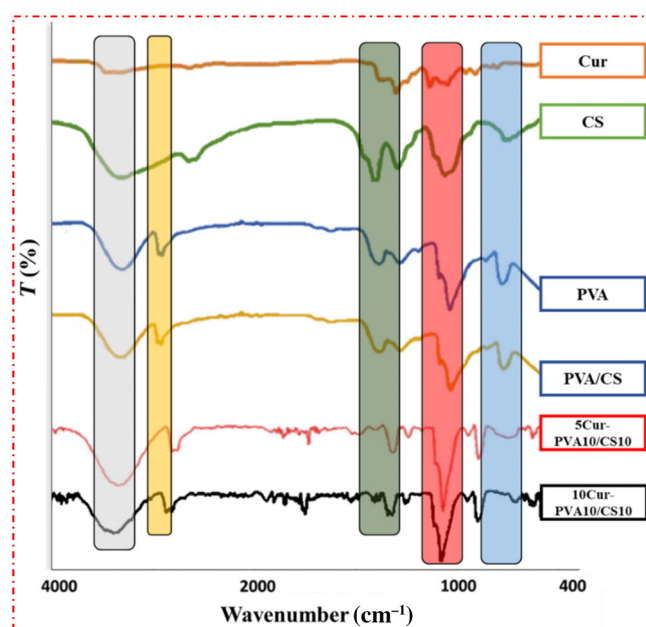

FIGURE 2 Fourier transform infrared spectra of the polyvinyl alcohol (PVA), chitosan (CS), curcumin (Cur), and Cur-loaded transdermal composite mats. [Color figure can be viewed at wileyonlinelibrary.com]

pure CS amino groups is associated with peaks at 1439 and 1593 cm^{-1} and C=O vibrational bands at 1658 cm^{-1}. The peak at 1439 cm^{-1} refers to carboxylic acid, and the peak around 1593 cm^{-1} is associated with the symmetric deformation of —$NH3^+$ groups.[40–42] In addition, the peaks are assigned to C—C at 1375 cm^{-1}, C—N at 1159 cm^{-1}, and C—O stretching peaks at 1042 cm^{-1}, respectively.[43]

3.4 | In vitro behaviors of transdermal composite mats

The evaluation of swelling behavior in mats is of great significance in skin tissue engineering. The findings of the investigation demonstrated that there were discrepancies in the swelling characteristics of the mats. In contrast, the Cur-loaded composite mats had a greater capacity for swelling than the PVA mat. The observed increase in swelling behavior may be ascribed to various functional groups within natural materials.[44] Combining PVA with CS and Cur in the fibers improved hydrophilic properties compared with pure PVA mats. Furthermore, the electrostatically charged Cur increased the free functional groups within the mats. The incorporation of Cur in the mats correlated with enhanced water retention capacity, resulting in a swelling of the mats ranging from 55% to over 100% within a specific time frame (Figure 3a). The rate of change in the swelling ratio graphs for composite mats loaded with Cur generally exhibited a positive correlation with time. This observation aligns with the results reported in previous research, which have demonstrated that the swelling properties of Cur are enhanced when mixed with different substances.[45,46] As fibers swell, their surface area typically increases, which leads to more significant cell infiltration and attachment. Consequently, incorporating Cur further expanded the network, facilitating easier water infiltration and a higher degree of swelling. It is anticipated that there exists an inverse correlation between the degradation of composite mats and the rate at which tissue regeneration occurs. In skin tissue engineering, it is critical that the biomaterial endures complete degradation solely after the proliferative phase of wound healing has concluded.[8,11] The highest swelling was observed in the PVA10/CS10 mat while the lowest degradation was also observed in the PVA10/CS10. On the initial day of the trial, PVA10 experienced a weight reduction of nearly 90%. Nevertheless, the rate at which it degraded exhibited a steady decrease over time, following the pattern observed in other composite materials (Figure 3b). In contrast, it was observed that the composite mats containing 5Cur-PVA10/CS10 displayed the most minimal

degradation rate compared with PVA10 and 10Cur-PVA10/CS10. The inclusion of Cur (up to 5%) in the composite mat resulted in a noticeable reduction in the degradation rate of the composite mats. This characteristic is favorable for long-term skin tissue engineering applications, as it suggests that the composite mat would maintain its structural integrity during the critical phases of tissue regeneration. The observed alteration in swelling behavior may be attributed to reduced accessibility of the hydrophilic functional group inside the composite mats. A decrease in the concentration of free hydrophilic groups may be accompanied by the reduction in the swelling value of the composite mats. This may be attributed to the creating of a cross-linked and stiff network through intermolecular and intramolecular bonding. The primary cause of the swelling behavior observed in the composite mats was the enhanced binding of the amine groups of CS in the PVA10/CS10 composite mats through crosslinking with GA. At the same time, the swelling rate (%) of the 10Cur-PVA10/CS10 sample was lower than the swelling rate (%) of 5Cur-PVA10/CS10 sample. This result may be related to the increased concentration of hydrophobic Cur in the composite mat.[47,48]

Following 24 h, it was determined that approximately 50% of the Cur was released from every composite mat. Compared with the 5Cur-PVA10/CS10 composite mats, the release of CUR is more rapid in the 10Cur-PVA10/CS10 composite mats, as indicated in Table 3. This phenomenon is expected to increase systemic bioavailability and improve in vivo efficacy. The solubility of Cur in water and its influence on the cellular activity of composite mats make it necessary to control its release closely. Therefore, measuring the amount of released Cur is essential in evaluating materials. Higher composite loadings are associated with a faster and more considerable release. The observed phenomenon can be attributed to an elevated concentration of Cur, resulting in a more pronounced concentration gradient. Consequently, this creates a more substantial diffusion driving force, which promotes the release process. The release rate of 5Cur-PVA10/CS10 from mats was higher than other mats loaded with Cur. Following 48 h, it was observed that only 63% of Cur was released from the 10Cur-PVA10/CS10 mats, suggesting a sustained release in an in vitro setting. The Cur delivery profile may be divided into two separate phases: a first stage lasting 24 h characterized by a fast release of the bioactive substance, followed by a secondary period lasting 48 h where the bioactive material is dispensed in a protracted and sustained way. The primary aim of controlled release systems is to maintain a specific biomolecule concentration at the intended site of action over an extended period. These systems are generally activated by administering a fraction of the
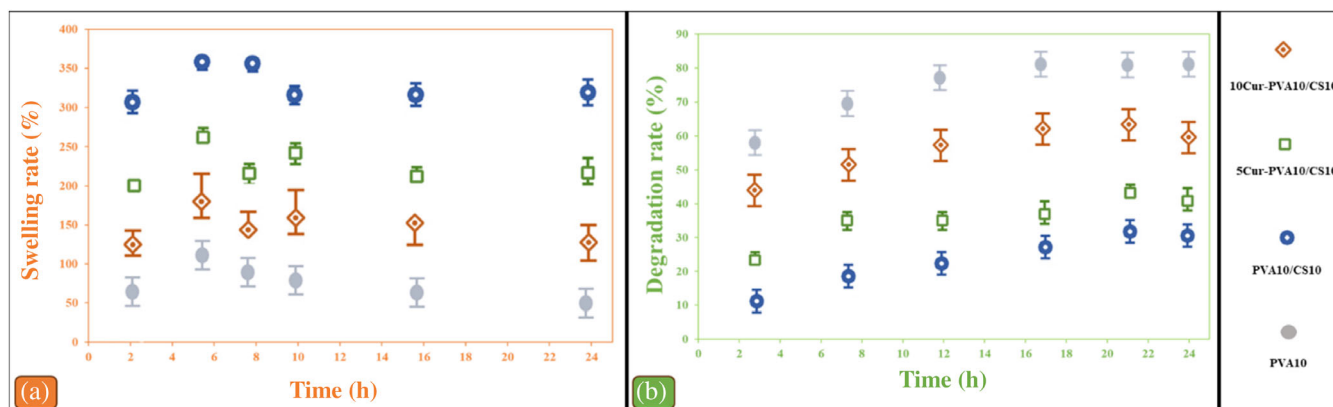
FIGURE 3 (a) Swelling and (b) degradation behavior profiles of the transdermal composite mats. [Color figure can be viewed at wileyonlinelibrary.com]

complete dosage to rapidly achieve the desired therapeutic biomolecule concentration. Following this, the release profile of the bioactive material exhibits a predetermined pattern, ensuring a continuous supply of the required dosage to sustain the optimal concentration of the bioactive material. Release kinetic behavior of Cur-loaded transdermal composite mats was studied with different kinetic models. The effectiveness of the different release profiles was assessed using the correlation coefficient (R^2). The mathematical model with the highest degree of correlation coefficient was deemed the most appropriate description of the Cur release kinetics. The results of release kinetic behavior of Cur-loaded transdermal composite mats may be given for 5Cur-PVA10/CS10, first-order mathematical model correlation coefficient; k; $0.023/R^2$; 0.83, zero-order mathematical model coefficients; k; $0.007/R^2$; 0.71, Higuchi mathematical model coefficients; k; $0.086/R^2$; 0.97, Korsmeyer-Peppas mathematical model coefficients; k; $0.02/R^2$; 0.9832, n; 0.79 (Table 3), and 10Cur-PVA10/CS10, first-order mathematical model correlation coefficient; k; $0.023/R^2$; 0.75, zero-order mathematical model coefficients; k; $0.007/R^2$; 0.78, Higuchi mathematical model coefficients; k; $0.082/R^2$; 0.93, Korsmeyer-Peppas mathematical model coefficients; k; $0.011/R^2$; 0.9884, n; 0.82 (Table 3). The findings from the examination of the first-order model applied to the 5Cur-PVA10/CS10, and 10Cur-PVA10/CS10 composite mats suggested that the mechanism of biomolecule release exhibited non-Fickian behavior and adhered to a release type characterized by anomalous diffusion-controlled release.[49] The observed release profile exhibited a combination of biomolecule release mechanisms, specifically diffusion-controlled and swelling-controlled release. The collective findings from the release studies demonstrated that the composite mats conjugated with Cur are well-suited for delivering consistent and prolonged quantities of Cur. The primary release of

medication will function as an initial dose, effectively managing the dissemination of the illness, while the prolonged release stage will lead to enhanced therapeutic results.

In the real world of biomolecule release and dissolution kinetics, a range of parameters and equations serve to elucidate the patterns of biomolecule release. These include "C_t," denoting the concentration of the active agent released at a particular time "t," and "C_0," signifying the initial concentration of the active agent at the start of dissolution (often presumed to be zero). The "K_0" constant characterizes zero-order drug release, maintaining a constant rate throughout. "Q_1" represents the amount released at time "t," with "Q_0" as the initial drug quantity. "K_1" embodies the rate of first-order biomolecule release, where the rate diminishes exponentially with time. "K_H" pertains to the _Higuchi model_, modeling drug release as a square root of a time-dependent process. "M_∞" stands for the maximum achievable drug release at equilibrium, while "M_i" designates the drug amount released at a specified time "t." "K_r" reflects the release velocity constant linked to structural and geometric attributes of the system, and "n" is the release exponent indicating how the release rate changes over time. "l" signifies the latency time, and "b" denotes the burst effect, where an initial surge of biomolecule release occurs in specific delivery systems. These parameters and models play a pivotal role in pharmacokinetics and pharmaceutical sciences, facilitating the comprehension and control of biomolecule release dynamics from diverse delivery systems for therapeutic applications. In order to assess the release kinetics mechanism of Cur, the concentration of the released Cur was subjected to fitting equations proposed by the Higuchi model and Korsmeyer-Peppas.[50] Fick's law predicts that a diffusion-controlled mechanism will produce a linear graph when the bioactive molecule is delivered.[51,52] As

TABLE 3 Cur release profiles with different models and loading efficiency values of Cur-loaded transdermal composite mats.

| Composite mats	Kinetic models	Linear equations	Equations	Coefficients, buffer pH 7.4			Loading efficiency (LE)
				K (K_0, K_1, K_H and K_r)	R^2	n	%
5Cur-PVA10/CS10	Zero order	$y = 0.0623x - 0.0016$, $R^2 = 0.99$	$C_t = C_0 + K_0 t$	6.70×10^{-9}	0.719		88.41 ± 0.72
	First order		$\log Q_1 = \log Q_0 + K_1 t / 2.303$	2.30×10^{-11}	0.835		
	Higuchi		$f_t = Q = K_H t^{1/2}$	8.60×10^{-7}	0.978		
	Korsmeyer-Peppas (power law)		$M_t / M_\infty = K_r t^n + b$	2.42×10^{-9}	0.983	0.79	
10Cur-PVA10/CS10	Zero order	$y = 0.0635x + 0.0038$, $R^2 = 0.99$	$C_t = C_0 + K_0 t$	6.80×10^{-9}	0.786		96.16 ± 2.75
	First order		$\log Q_1 = \log Q_0 + K_1 t / 2.303$	2.24×10^{-11}	0.754		
	Higuchi		$f_t = Q = K_H t^{1/2}$	8.20×10^{-7}	0.938		
	Korsmeyer-Peppas (power law)		$M_t / M_\infty = K_r t^n + b$	1.10×10^{-9}	0.988	0.82	

Abbreviations: Cur, curcumin; CS, chitosan; PVA, polyvinyl alcohol.

evidenced in the concluding sections of the two models, the release profiles encompass two distinct stages within each model. The data reveal strong linear connections ($R^2 \geq 0.978$) between the release rate and $t_{1/2}$ for the initial and subsequent stages. Notably, the first stage exhibits a steeper slope than the second. The phenomenon can be clarified in the following manner: molecules of bioactive compounds situated close to the surface of the composite mats or weakly attached to the surface exhibit a higher diffusion rate and are liberated during the first timeframe. During the subsequent release stage, the bioactive substance molecules within the composite mats' interior require a prolonged duration to migrate toward the surface, which entails destroying specific polymer units. Consequently, the rate of release is decelerated. The dissolution of polymers typically encompasses the processes of water absorption, swelling, and dissolution. Composite mats designed for the controlled release of bioactive chemicals are predominantly fabricated during the initial two phases, adsorption, and swelling, corresponding to the release profile's initial phase. In contrast, it is shown that most composite mats undergo structural degradation due to polymer erosion during the subsequent phase. Hence, it is probable that a combination of diffusion and erosion mechanisms governs the controlled release of the bioactive molecule.

3.5 | Antioxidant activity of transdermal composite mats

The composite mats' antioxidant activity was assessed using the DPPH radical scavenging method.[53] As depicted in Figure 4, both Cur, 5Cur-PVA10/CS10, and 10Cur-PVA10/CS10 exhibited antioxidant capabilities. This finding suggests that Cur can maintain its effective antioxidant performance even under high electrified force conditions.[54] Notably, 10Cur-PVA10/CS10 demonstrated superior antioxidant ability compared with 5Cur-PVA10/CS10, with a radical scavenging activity of 86.941 $\pm$ 0.02 (%) observed when the concentration of Cur increased to 0.02 mg/mL in composite mats. The heightened antioxidant activity of 10Cur-PVA10/CS10 can be attributed to the increased water-solubility of Cur, followed by CS crosslinking.[55] In previous research, nanocomposites have been prepared using various formulations that involve the encapsulation of Cur within combinations of CS, sodium alginate (ALG), and PVA for application in advanced drug delivery systems. These designed nanocomposites were subjected to DPPH free radical scavenging activity assays to assess their antioxidant capabilities. Remarkably, while free Cur exhibited an antioxidant activity of around 72.29%, the Cur-loaded nanocomposites displayed even more significant antioxidant potential. Precisely, the antioxidant activities of Cur/Cs, Cur/Cs-ALG, Cur/Cs-PVA, and Cur/Cs-ALG-PVA were calculated as 79.6%, 81.14%, 82.96%, and 85.79%, respectively.[56] Similarly, in another investigation, Cur nanocarriers were incorporated into pectin (PEC), β-cyclodextrin (β-CD), AL, and PVA polymers utilizing the ionic gelation technique with nano-sized CS. Notably, Cur/Cs-PVA and Cur/CS demonstrated 76% and 72% antioxidant activities, respectively. These findings affirm that Cur effectively retains its valuable antioxidant properties following encapsulation within these innovative delivery systems.[54] The
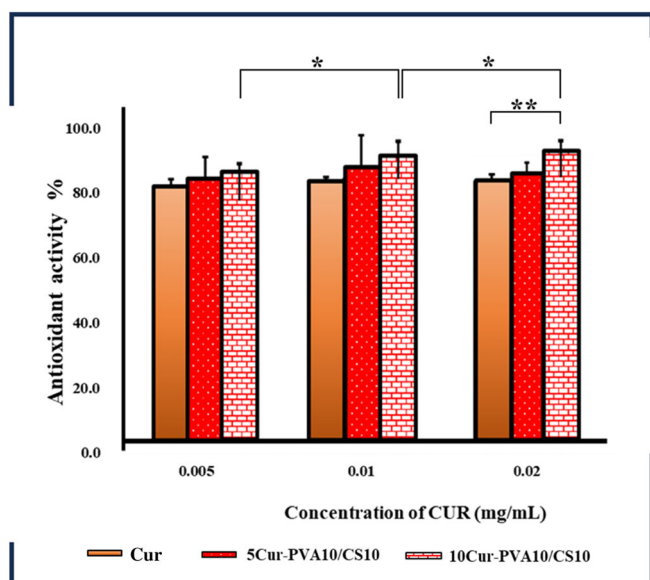
FIGURE 4 Antioxidant ability of Cur, 5Cur-PVA10/CS10, and 10Cur-PVA10/CS10 (*, ** statistical significance level was determined as $p < 0.05$ and the parenthesis indicates standard deviation). Cur, curcumin; CS, chitosan; PVA, polyvinyl alcohol. [Color figure can be viewed at wileyonlinelibrary.com]

antioxidant activity of Cur depends on its phenolic hydroxyl group. The phenoxy group in composite mats containing CS and Cur revealed antioxidant activity by carrying hydrogen atoms to free radicals. The results of the antioxidant activity of the transdermal composite mats showed that Cur retained its free radical activity even after loading into fibers by electrospinning and freeze-drying. Thus, it was concluded that the antioxidant activity of Cur (5%–10%)-loaded PVA10/CS10 transdermal composite mats was more effective (Figure 4).

3.6 | Antimicrobial activity of transdermal composite mats

The Supplementary S1 provided photos displaying the antibacterial activity of the Cur-loaded composite mats. All of the composite mats exhibited promising antibacterial effects against both microorganisms. According to the data presented in Table 4, the 10Cur-PVA10/CS10 composite exhibited a maximum zone of inhibition of 10.23 mm against *S. aureus*. In contrast, the PVA10/CS10 composite displayed a minimum zone of inhibition of 8.32 mm against the same bacteria. On the other hand, the 10Cur-PVA10/CS10 had a higher contact inhibition value than PVA10/CS10 when tested against *E. coli*. Adding Cur to PVA10/CS10 demonstrated effectiveness against *E. coli*, as evidenced by the increased inhibition value. The findings of this study align with previous

TABLE 4 The antimicrobial activity results of the control group and Cur-loaded transdermal composite mats.

| Samples	*Staphylococcus aureus* (ATCC 29213) (inhibition zone, mm)
PVA10 (control)	8.03 ± 0.16[*]
PVA10/CS10	8.32 ± 0.1[*]
5Cur-PVA10/CS10	9.56 ± 0.16[*]
10Cur-PVA10/CS10	10.23 ± 0.32[*]

Abbreviations: Cur, curcumin; CS, chitosan; PVA, polyvinyl alcohol.
*Statistical significance level was determined as $p < 0.05$.

research,[57] which has shown that Cur exhibits antibacterial properties against *E. coli*. The results of this study further corroborated the idea that bactericidal has a significant inhibitory effect on the growth of two indicator bacteria. The findings demonstrated that all composite mats exhibited antibacterial properties against Gram-positive and Gram-negative bacteria, indicating their potential application in skin tissue engineering, specifically for wound dressing.

In earlier studies, the compound Cur (curcumin was extracted from the rhizome of *Curcumi longa*) was subjected to cross-linking with CS-PVA membranes to explore its potential in wound healing. The agar well diffusion sensitivity method was employed to assess the antibacterial efficacy of Cur in isolation and combination with CS-PVA against a range of Gram-positive and Gram-negative bacteria. The study found that the Cur-CS-PVA membranes showed notable antibacterial activity against various microbes, including *E. coli, Pasturellamu ltocida, Bacillus subtilis*, and *S. aureus*.[16] Previous research has conducted in vitro–in vivo investigations on the efficacy of arginine-modified CS/PVA hydrogel-based microneedles (MNs) as delivery vehicles for Cur in the context of tissue engineering wound healing applications. The antibacterial efficacy of CUR-MN patches was assessed against Gram-positive (*S. aureus*) and Gram-negative (*E. coli*) bacterial strains by utilizing the agar well diffusion technique. The experimental findings demonstrated that CUR-MNs exhibit remarkable antibacterial efficacy against *S. aureus* and *E. coli*.[55]

3.7 | In vitro cell studies of transdermal composite mats

Figure 5a presents the data on the proportion of L929 cells that adhered to the surface of the specimens within
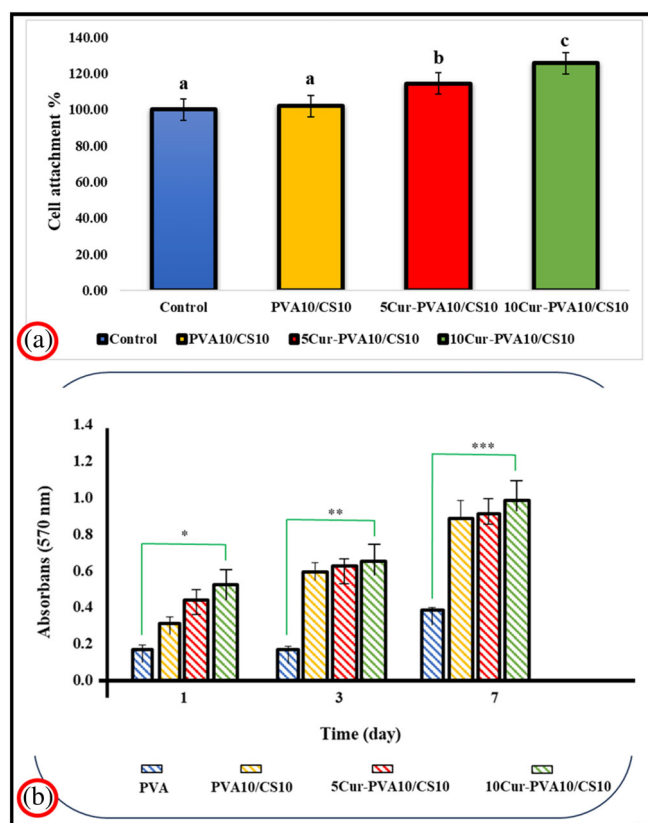
FIGURE 5 (a) Cell attachment (%) on transdermal composite mats, (b) cell viability of L929 cells after cytotoxicity tests of transdermal composite mats (*, **, ***, a, b, c statistical significance level was determined as $p < 0.05$). Cur, curcumin; CS, chitosan; PVA, polyvinyl alcohol. [Color figure can be viewed at wileyonlinelibrary.com]

24 h. The observed cell attachment % on the surfaces of PVA10/CS10 composite mats and the composite mats with the addition of Cur were significantly greater than those on pure PVA mats. The adhesiveness of L929 cells was shown to be higher on the surfaces of the composite mats (5Cur-PVA10/CS10 and 10Cur-PVA10/CS10) compared with PVA10 and PVA10/CS10. No relationship was observed between composite mats loaded with Cur. Nevertheless, the experimental group 10Cur-PVA10/CS10 had the most significant cell attachment rate. PVA10 is a naturally hydrophilic synthetic polymer with advantageous properties for facilitating cell adhesion. However, the propensity for proteins is diminished, impacting cellular adhesion's efficacy.[58] In addition, incorporating CS into the composite mat structure, together with PVA, led to an enhancement in hydrophilicity. This may be attributed to extra hydroxyl and amine groups from CS.[59] Moreover, the presence of functional groups such as hydroxyl, carbonyl, oxygen, and sulfates in Cur enhances the ability of the scaffolds to interact with proteins, leading to an increase in hydrophilicity. In this work, the impact of hydrophilicity on cell attachment was assessed by examining the impacts of both Cur and CS10. Upon careful examination, it was observed that the inclusion of Cur in PVA10/CS10 resulted in a slight enhancement in the number of cells stuck to the surfaces. Upon closer examination, it becomes evident that the composite mat designated as 10Cur-PVA10/CS10 exhibits the maximum ability for cell attachment. Cell viability was assessed using the MTT assay on cell culture's first, third, and seventh days, as presented in Figure 5b. Cell viability and cytotoxicity were evaluated for all composite mats, and no cytotoxic effects were observed for any of the composite mats over the course of 7 days. During these days, tissue culture polystyrene (TCPS) and PVA10 exhibited relatively close absorbance values. However, the absorbance values for PVA10 were consistently higher than those for TCPS throughout the 7-day culture period. It is worth noting that the addition of CS10 significantly enhanced the biocompatibility of the composite mats compared with PVA10 on all days of the study. This improvement in biocompatibility suggests that the presence of CS10 in the composite mats is conducive to cell viability and growth. In line with the findings related to cell attachment, the inclusion of Cur in 5Cur-PVA10/CS10 did not significantly impact cell viability. This observation confirms that the composite mats loaded with Cur did not exhibit cytotoxic properties. Furthermore, it was observed that the Cur-loaded transdermal composite mats had superior viability and cell proliferation results compared with the PVA10 and control groups. On the seventh day of the experiment, the transdermal composite mat labeled 5Cur-PVA10/CS10 exhibited the highest absorbance value compared with the control group and the other composite mats. In previous investigations involving PVA/CS nanofibers loaded with Cur, it was observed that these scaffolds facilitated the survival and growth of stem cells.[34] The primary objective of a prior investigation was to develop a targeted drug delivery system for breast and liver cancer. This was accomplished by constructing a membrane composed of polyvinyl alcohol/cellulose nanocrystals (PVA/CNCs) loaded with Cur. The MTT assay thoroughly assessed the efficiency of the PVA/CNCs/Cur membrane to measure its in vitro cytotoxicity. The findings demonstrated that the membrane had a concentration-dependent selective suppression of cell proliferation in breast and liver cancer cells. In contrast, it was seen that normal cells did not experience any changes, thereby highlighting the promise of this approach for precise cancer treatment.[49] Researchers developed composite materials in a related study area by combining polyvinyl alcohol/sodium alginate (PVA-SA) and Cur and adding graphene oxide (GO). These materials were created utilizing solvent casting
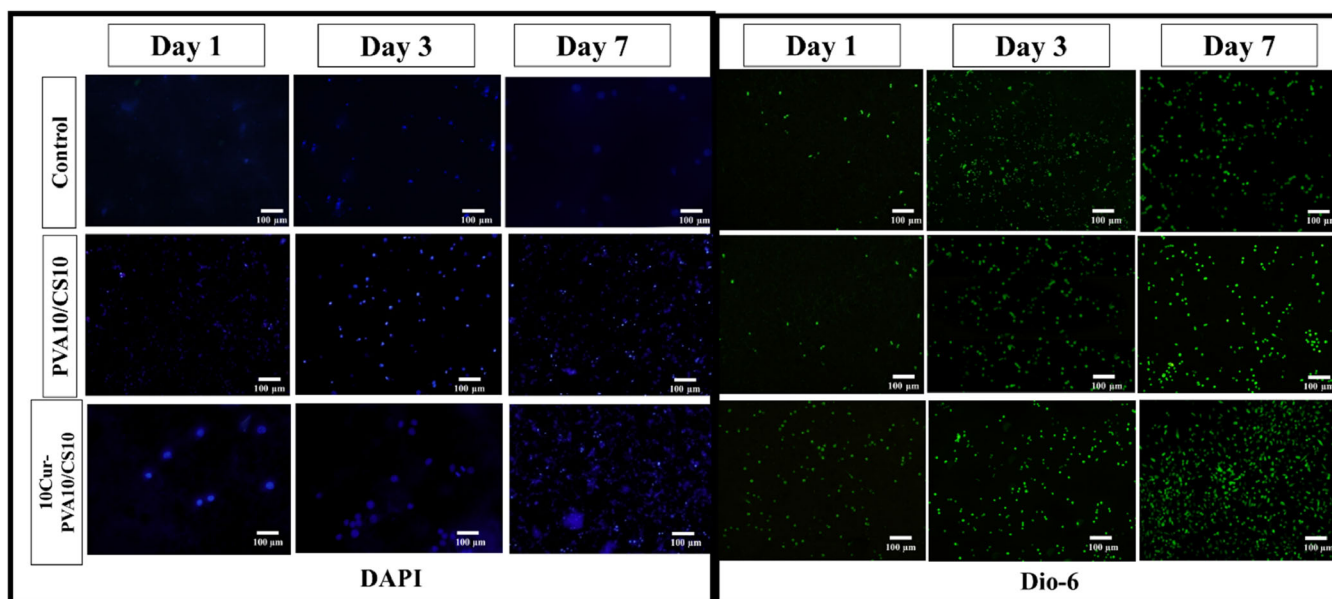
FIGURE 6 Florescence micrographs of the cells on the transdermal composite mats at the end of 1, 3, and 7 days stained with DAPI and Dio-6. Cur, curcumin; CS, chitosan; PVA, polyvinyl alcohol. [Color figure can be viewed at wileyonlinelibrary.com]

and electrospinning methods. The anticancer effectiveness of these novel drug delivery methods was evaluated by conducting the MTT assay on MCF-7 cells. The study found that the PVA-SA/GO 1 wt%-Cur film and PVA-SA/GO 10 wt%-Cur mat showed significant promise as drug delivery systems, indicating their potential for use in anticancer treatments.[60]

DAPI is highly specific for staining cell nuclei and generally does not label the cytoplasm. In this study, DAPI was used to stain the nuclei of all fixed cells, and its blue color was observed under fluorescence microscopy. This staining revealed that in mats, there were indications of cell death, with the nuclei of these cells appearing disrupted. Figure 6 illustrates dead cells within the mats. The PVA10/CS10 composite mat did not appear to support sufficient cell proliferation, but an increase in the amount of Cur resulted in improved cell proliferation and attachment. These findings suggest that the loading of Cur may enhance cell proliferation and attachment within the composite mats, potentially making it more suitable for tissue engineering applications. Similar Cur-loaded studies have also shown that the engineered scaffolds are not cytotoxic and promote cell proliferation.[61] The dyes in this study labeled neurons through lateral diffusion on the plasma membrane in fixed samples. This labeling process is faster in living tissue due to active dye transfer processes. In this particular study, Dio-6 was employed to assess the endoplasmic reticulum's activity and determine the extent of cell grafting and proliferation, particularly concerning the use of Cur. As depicted in Figure 6, the endoplasmic reticulum of cells loaded

with 10Cur appeared more active and healthier than others. Furthermore, cell activations were quite good overall, but when making comparisons, the loading of Cur appeared to have a significant positive impact on cell adhesion. This suggests that incorporating Cur into the system significantly contributes to cell adhesion and potentially enhances overall cell health and activity. In previous Cur-loaded PVA/CS film studies, it was observed that cell adhesion occurred as a result of cell nucleus staining.[62] The scratch assay involving fibroblast cells was conducted to evaluate the influence of mats on cell migration and wound healing capabilities. Fibroblast cells are pivotal in the proliferative phase of wound healing due to their capacity to migrate, contract, proliferate, and synthesize collagen. Figure 7 displays microscope images of scratches treated with PVA10/CS10 (Figure 7b) and 10Cur-loaded PVA10/CS10 (Figure 7c) composite mats, along with a control (Figure 7a), at 0, 12, and 24 h. Upon examination of the results, it is evident that PVA10/CS10 and 10Cur-PVA10/CS10 composite mats were highly effective in promoting scratch closure compared with the control group by the end of the 12th hour. The most notable improvement was observed in the study involving the treatment with 10Cur-PVA10/CS10 at the end of 24 h (Figure 7d). In similar studies, Cur-loaded PVA nanofiber membranes were observed to be sufficiently effective in an in vitro scratch wound healing assay.[63] After 24 h, the study observed the highest rate of scratch closure on the 10Cur-PVA10/CS10 composite mats. The closure rate on the PVA10/CS10 composite mats was nearly similar to that of the

FIGURE 7 (a–c) In vitro wound healing activity cell migration into the scratch area after 0–12–24 h for the transdermal composite mats and (d) wound closure efficiency (healing ability) for the transdermal composite mats (*, ** statistical significance level was determined as $p < 0.05$). Cur, curcumin; CS, chitosan; PVA, polyvinyl alcohol. [Color figure can be viewed at wileyonlinelibrary.com]
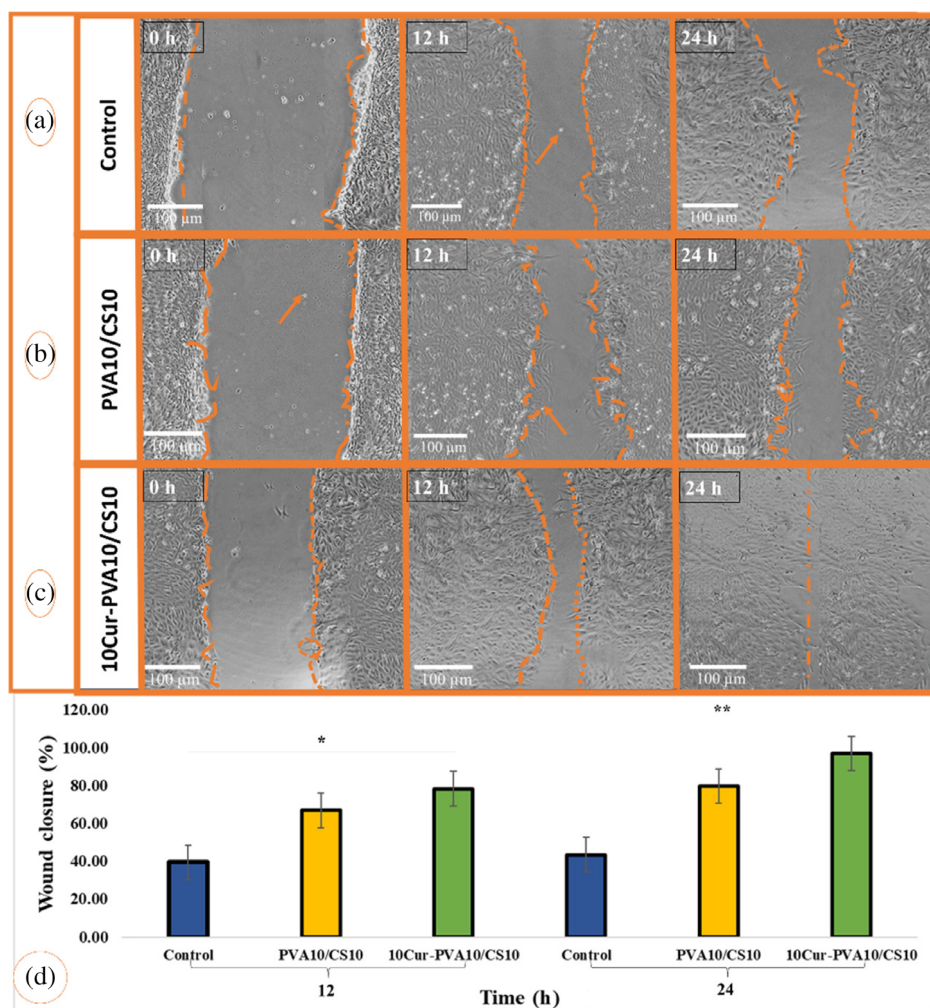
10Cur-PVA10/CS10 composite mats and the control group. These results indicate that the 10Cur-PVA10/CS10 composite mats yielded the most significant and clear scratch closure outcomes. Based on the findings from DAPI and Dio-6 cell line staining, as well as the scratch closure results, it can be concluded that the incorporation of Cur, a bioactive substance, into the 10Cur-PVA10/CS10 composite mats, as well as PVA10/CS10 composite mats, enhances the migration of fibroblast cells and expedites wound closure. In similar studies, PVA/CS nanofibrous mats were observed to be sufficiently effective *in* in vitro scratch assay wound healing.[64] Obtained results showed that Cur may be an effective wound-healing accelerator in wound dressings. These results hold promise for developing wound dressings that can facilitate and expedite the wound-healing process. Furthermore, the results showed that the increased surface roughness of the cross-linked transdermal composite mats may increase cell adhesion.[65–67] Thus, this feature may make the cross-linked transdermal composite mats a viable candidate for wound healing applications.[68–70]

4 | CONCLUSION

The study obtained PVA, PVA/CS, and PVA/CS/Cur solutions as fiber materials by electrospinning method. Transdermal composite mats were produced by crosslinking the fibers by steaming, freezing, and drying. The Cur (bioactive molecule) exhibited enhanced retention capacity, biocompatibility, superior mechanical qualities, and biodegradability when used at low concentrations. The observed augmentation in hydrophobicity demonstrated effective release kinetics and facilitated wound healing through the stimulation of cellular proliferation. The transdermal composite mats loaded with Cur exhibited enhanced antioxidant activity, surpassing 80% and reaching higher levels. A biocompatibility assay was conducted on fibroblast cells in order to assess and compare the extent of cell proliferation on transdermal composite mats. Because of the increased intermolecular bonding between the polymeric chains in the composite mats, the surface roughness increased significantly after crosslinking, which aligns with the literature. The increase in surface

roughness facilitates cell adhesion and is a favorable property for wound healing applications. The study also showed that Cur-loaded composite mats exhibited a significant increase in fibroblast adhesion and proliferation, as demonstrated by DAPI and Dio-6 fluorescence staining. The composite mats that exhibited the highest cell adhesion were the 5Cur-PVA10/CS10 and 10Cur-PVA10/CS10 composite mats. These mats demonstrated morphological characteristics that were compatible with fibroblast-like cells. In addition, the composite mats loaded with Cur demonstrated notable antibacterial efficacy against various harmful bacterial strains, such as *E. coli* and *S. aureus*. Furthermore, the staining assessments demonstrated that the composite mats of PVA10/CS10 loaded with Cur had remarkable cell viability values. Furthermore, the 10Cur-PVA10/CS10 composite mat exhibited the most rapid rate of scratch closure. Notably, these mats displayed the most significant degree of closure after 24 h compared with the other composite mats under investigation. The utilization of Cur not only affords protection for the loaded active substance but also may enhance its potency and increase the efficacy of the treatment. Because of its multifaceted characteristics and extensive scope for possible utilization, Cur-loaded polymer composite mats are anticipated to attract growing attention within the biomedicine, pharmaceutical, and biomedical sectors.

AUTHOR CONTRIBUTIONS

ACKNOWLEDGMENTS

FUNDING INFORMATION

DATA AVAILABILITY STATEMENT

ORCID

Fatih Ciftci https://orcid.org/0000-0002-3062-2404
Ali Can Özarslan https://orcid.org/0000-0002-4864-0598
Nilüfer Evcimen Duygulu https://orcid.org/0000-0003-4651-750X

REFERENCES

[1] S. Ali, M. Shabbir, N. Shahid, *Res. J. Pharm. Technol.* **2015**, *8*, 103.
[2] D. Bird, N. M. Ravindra, *Med. Devices Sens.* **2020**, *3*, e10069.
[3] A. Zoabi, E. Touitou, K. Margulis, *Colloids Interfaces* **2021**, *5*, 18.
[4] C. Y. Kadam, A. Muchandi, P. P. Alabade, P. P. Narwade, S. R. Khandwe, *Int. J. Sci. Dev. Res.* **2022**, *7*, 123.
[5] L. Liu, W. Zhao, Q. Ma, Y. Gao, W. Wang, X. Zhang, Y. Dong, T. Zhang, Y. Liang, S. Han, J. Cao, X. Wang, W. Sun, H. Ma, Y. Sun, *Nanoscale Adv.* **2023**, *5*, 1527.
[6] Y. B. Elalmis, E. Tiryaki, B. K. Ikizler, S. Yucel, *Micro- and Nanoengineered Gum-Based Biomaterials for Drug Delivery and Biomedical Applications*, Elsevier, Amsterdam, Netherlands **2022**, p. 303.
[7] K. N. Durga, P. Bhuvaneswari, B. Hemalatha, K. Padmalatha, *Asian J. Pharm. Technol.* **2022**, *12*, 159.
[8] F. Ciftci, *Int. J. Biol. Macromol.* **2023**, *235*, 123769.
[9] M. Sikandar, M. H. Shoaib, R. I. Yousuf, F. R. Ahmed, F. R. Ali, M. T. Saleem, K. Ahmed, S. Sarfaraz, S. Jabeen, F. Siddiqui, T. Husain, F. Qazi, M. S. Imtiaz, *Int. J. Nanomed.* **2022**, *17*, 3463.
[10] A. Yilmaz, *Emerging Mater. Res.* **2021**, *10*, 158.
[11] F. Ciftci, A. C. Özarslan, *J. Sol-Gel Sci. Technol.* **2023**, *109*, 192.
[12] B. Coşkuner Filiz, Y. Basaran Elalmis, İ. S. Bektaş, A. Kantürk Figen, *Int. J. Biol. Macromol.* **2021**, *192*, 999.
[13] S. M. Abdel-Hafez, R. M. Hathout, O. A. Sammour, *Int. J. Biol. Macromol.* **2018**, *108*, 753.
[14] R. S. Nair, A. Morris, N. Billa, C. O. Leong, *AAPS PharmSciTech* **2019**, *20*, 13.
[15] A. Erarslan, C. Y. Karakas, F. Bozkurt, O. Sagdic, *ChemistrySelect* **2023**, *8*, 1.
[16] M. Abbas, T. Hussain, M. Arshad, A. R. Ansari, A. Irshad, J. Nisar, F. Hussain, N. Masood, A. Nazir, M. Iqbal, *Int. J. Biol. Macromol.* **2019**, *140*, 871.
[17] K. Vimala, M. M. Yallapu, K. Varaprasad, N. N. Reddy, S. Ravindra, N. S. Naidu, K. M. Raju, *J. Biomater. Nanobiotechnol.* **2011**, *2*, 55.
[18] C. Keçeciler-Emir, Y. Başaran-Elalmiş, Y. M. Şahin, E. Buluş, S. Yücel, *Biopolymers* **2023**, *114*, e23562.
[19] M. Urošević, L. Nikolić, I. Gajić, V. Nikolić, A. Dinić, V. Miljković, *Antibiotics* **2022**, *11*, 135.
[20] S. J. Stohs, O. Chen, S. D. Ray, J. Ji, L. R. Bucci, H. G. Preuss, *Molecules* **2020**, *25*, 1397.
[21] Y. Hussain, W. Alam, H. Ullah, M. Dacrema, M. Daglia, H. Khan, C. R. Arciola, *Antibiotics* **2022**, *11*, 322.

[22] R. Tabanelli, S. Brogi, V. Calderone, *Pharmaceutics* **2021**, *13*, 1715.

[23] Z. Li, M. Shi, N. Li, R. Xu, *Application of Functional Biocompatible Nanomaterials to Improve Curcumin Bioavailability. Front. Chem.* **2020**, *8*, 589957.

[24] A. C. Mendes, C. Gorzelanny, N. Halter, S. W. Schneider, I. S. Chronakis, *Int. J. Pharm.* **2016**, *510*, 48.

[25] Y. Liu, S. Wang, R. Zhang, *Int. J. Biol. Macromol.* **2017**, *103*, 1130.

[26] B. I. Tarnowski, F. G. Spinale, J. H. Nicholson, *Biotech. Histochem.* **1991**, *66*, 296.

[27] P. Kerrison, & M. Steinke, DAPI staining protocol. Private www.Essex.Ac.Uk, m(December), **2010**, 4.

[28] H.-Y. Chang, H.-C. Huang, T.-C. Huang, P.-C. Yang, Y.-C. Wang, H.-F. Juan, *Bio-Protoc.* **2013**, *3*, e431.

[29] P. J. Babu, M. Doble, A. M. Raichur, *J. Colloid Interface Sci.* **2018**, *513*, 62.

[30] N. E. Duygulu, F. Ciftci, C. B. Ustundag, *J. Polym. Res.* **2020**, *27*, 232.

[31] A. Abraham, P. A. Soloman, V. O. Rejini, *Procedia Technol.* **2016**, *24*, 741.

[32] X. Z. Sun, G. R. Williams, X. X. Hou, L. M. Zhu, *Carbohydr. Polym.* **2013**, *94*, 147.

[33] M. E. Ostheller, A. M. Abdelgawad, N. K. Balakrishnan, A. H. Hassanin, R. Groten, G. Seide, *Nanomaterials* **2022**, *12*, 24.

[34] A. Golchin, S. Hosseinzadeh, M. Staji, M. Soleimani, A. Ardeshirylajimi, A. Khojasteh, *J. Cell. Biochem.* **2019**, *120*, 15410.

[35] P. Dubey, P. Gopinath, *RSC Adv.* **2016**, *6*, 69103.

[36] S. Ahmadi Majd, M. Rabbani Khorasgani, S. J. Moshtaghian, A. Talebi, M. Khezri, *Int. J. Biol. Macromol.* **2016**, *92*, 1162.

[37] M. M. Mahmud, S. Zaman, A. Perveen, R. A. Jahan, M. F. Islam, M. T. Arafat, *J. Drug Delivery Sci. Technol.* **2020**, *55*, 101386.

[38] S. Jiayin, G. Jing, W. Lu, *Chem. Fibers Int.* **2022**, *72*, 138.

[39] G. Ju, X. Liu, R. Li, M. Li, Z. Qin, X. Yin, *Colloid Polym. Sci.* **2021**, *299*, 1955.

[40] K. Paipitak, T. Pornpra, P. Mongkontalang, W. Techitdheer, W. Pecharapa, *Procedia Eng.* **2011**, *8*, 101.

[41] S. Wang, F. Yan, P. Ren, Y. Li, Q. Wu, X. Fang, F. Chen, C. Wang, *Int. J. Biol. Macromol.* **2020**, *158*, 9.

[42] N. N. Rupiasih, D. A. Sukma Pranastia, M. Sumadiyasa, P. B. Vidyasagar, *J. NeutrinoJurnal Fis. dan Apl.* **2023**, *15*, 62.

[43] L. Li, Y. L. Hsieh, *Carbohydr. Res.* **2006**, *341*, 374.

[44] T. Ngawhirunpat, P. Opanasopit, T. Rojanarata, P. Akkaramongkolporn, U. Ruktanonchai, P. Supaphol, *Pharm. Dev. Technol.* **2009**, *14*, 73.

[45] D. Lin, L. Xiao, W. Qin, D. A. Loy, Z. Wu, H. Chen, Q. Zhang, *Carbohydr. Polym.* **2022**, *281*, 119080.

[46] M. Heidarifard, E. Taghavi, N. Anarjan, *J. Am. Oil Chem. Soc.* **2021**, *98*, 697.

[47] G. Rezvan, G. Pircheraghi, R. Bagheri, *J. Appl. Polym. Sci.* **2018**, *135*, 46734.

[48] S. Rathinavel, J. Indrakumar, P. S. Korrapati, S. Dharmalingam, *Colloids Surfaces A Physicochem. Eng. Asp.* **2022**, *637*, 128185.

[49] Y. Hussein, S. A. Loutfy, E. A. Kamoun, S. H. El-Moslamy, E. M. Radwan, S. E. I. Elbehairi, *Int. J. Biol. Macromol.* **2021**, *170*, 107.

[50] J. X. Wang, Z. H. Wang, J. F. Chen, J. Yun, *Mater. Res. Bull.* **2008**, *43*, 3374.

[51] S. M. Huang, S. M. Liu, H. Y. Tseng, W. C. Chen, *Membranes* **2023**, *13*, 564.

[52] M. Rezaei, M. Nikkhah, S. Mohammadi, S. H. Bahrami, M. Sadeghizadeh, *J. Appl. Polym. Sci.* **2021**, *138*, 50884.

[53] A. Ullah, S. Ullah, M. Q. Khan, M. Hashmi, P. D. Nam, Y. Kato, Y. Tamada, I. S. Kim, *Int. J. Biol. Macromol.* **2020**, *155*, 479.

[54] A. Rezagholizade-shirvan, M. Masrournia, M. Fathi Najafi, H. Behmadi, *Polym. Bull.* **2023**, *80*, 1495.

[55] M. Hasnain, T. Kanwal, K. Rehman, S. R. U. Rehman, S. Aslam, T. Roome, S. Perveen, M. B. Zaidi, S. Saifullah, S. Yasmeen, A. Hasan, M. R. Shah, *Int. J. Biol. Macromol.* **2023**, *253*, 126697.

[56] A. Rezagholizade-shirvan, M. Fathi Najafi, H. Behmadi, M. Masrournia, *Inorg. Chem. Commun.* **2022**, *145*, 110022.

[57] S. K. Bajpai, N. Chand, S. Ahuja, *Int. J. Biol. Macromol.* **2015**, *79*, 440.

[58] M. A. M. Hussein, S. Su, S. Ulag, A. Woźniak, M. Grinholc, G. Erdemir, S. E. Kuruca, O. Gunduz, M. Muhammed, I. M. El-Sherbiny, M. Megahed, *Polymers* **2021**, *13*, 3630.

[59] M. A. Welchoff, A. T. Wittenberg, J. C. Jimenez, D. Kamireddi, E. K. Snelling, R. M. Street, C. L. Schauer, *Polym. Eng. Sci.* **1921**, *2023*, 63.

[60] Z. Mirzaie, A. Reisi-Vanani, M. Barati, S. M. Atyabi, *J. Pharm. Sci.* **2021**, *110*, 3715.

[61] M. Amirthalingam, N. Kasinathan, S. Mutalik, N. Udupa, *J. Microencapsulation* **2015**, *32*, 364.

[62] R. Ramdani, A. M. Rao, M. Pokharel, T. Mateti, K. Likhith, M. Kumari, S. S. Bhatt, G. Thakur, *JOM* **2023**, *75*, 5581.

[63] M. Roopesh, D. Davis, M. S. Jyothi, M. Vandana, B. S. Thippeswamy, G. Hegde, T. P. Vinod, R. S. Keri, *RSC Adv.* **2023**, *13*, 24320.

[64] H. Adeli, M. T. Khorasani, M. Parvazinia, *Int. J. Biol. Macromol.* **2019**, *122*, 238.

[65] C. N. Grover, J. H. Gwynne, N. Pugh, S. Hamaia, R. W. Farndale, S. M. Best, R. E. Cameron, *Acta Biomater.* **2012**, *8*, 3080.

[66] E. R. S. Kenawy, E. A. Kamoun, Z. S. Ghaly, A. Shokr, M. baset, M. A. El-Meligy, Y. A. G. Mahmoud, *Arabian J. Sci. Eng.* **2023**, *48*, 497.

[67] F. C. do Nascimento, L. C. V. de Aguiar, L. A. T. Costa, M. T. Fernandes, R. J. Marassi, A. d. S. Gomes, J. A. de Castro, *Polym. Bull.* **2021**, *78*, 917.

[68] N. Rashid, S. H. Khalid, I. Ullah Khan, Z. Chauhdary, H. Mahmood, A. Saleem, M. Umair, S. Asghar, *ACS Omega* **2023**, *8*, 7575.

[69] C. Li, J. Fei, T. Zhang, S. Zhao, L. Qi, *Composites, Part B* **2023**, *249*, 110422.

[70] S. Alven, X. Nqoro, B. A. Aderibigbe, *Polymers* **2020**, *12*, 1.

SUPPORTING INFORMATION

Additional supporting information can be found online in the Supporting Information section at the end of this article.